Using Boundary Conditions for Estimation of Complex Modulus From Flexural Wave Experiments

Kaushik Mahata, Saed Mousavi, Torsten Söderström, and Urmas Valdek

***Abstract*—Estimation of the complex Young's modulus from transverse wave experiment is considered in this brief. The main goal is to modify the usual least squares estimate so that additional information provided by the boundary conditions can be incorporated in the estimation algorithm. As a result, it is required to solve a constrained nonlinear least squares problem instead of an unconstrained one. The analytical results are validated using experimental data, where the modified estimates outperform the conventional nonlinear least squares estimate by a significant margin.**

***Index Terms*—Boundary condition, complex modulus, flexural waves, identification, nonlinear least squares, regularization, viscoelasticity.**

I. Introduction

FOR a linearly viscoelastic material, the stress $\sigma(t)$ at time instant t depends upon the entire deformation history and the relation between the stress and the strain can be expressed as

$$\sigma(t) = \int_{-\infty}^{t} Y(t-\tau)\dot{\varepsilon}(\tau)d\tau \tag{1}$$

where Y is the relaxation modulus and $\dot{\varepsilon}(t)$ is the time derivative of the strain $\varepsilon(t)$ [1], [2]. The convolution relationship in the time domain is equivalently expressed as a multiplication in frequency domain

$$\sigma'(\omega) = \mathcal{E}_\omega \varepsilon'(\omega) \tag{2}$$

where $\sigma'(\omega)$ and $\varepsilon'(\omega)$ are the Fourier transforms of $\sigma(t)$ and $\varepsilon(t)$, respectively.[1] The complex valued frequency dependent quantity

$$\mathcal{E}_\omega := \mathrm{i}\omega Y'(\omega) \tag{3}$$

Manuscript received March 24, 2004; revised December 20, 2004. Manuscript received in final form July 19, 2005. Recommended by Associate Editor G. Rosen. This work was supported by the Swedish Research Council for Engineering Sciences under Contract 2000-587.

K. Mahata is with the Centre for Complex Dynamic Systems and Control, University of Newcastle, Callaghan, NSW-2308, Australia (e-mail: Kaushik.Mahata@newcastle.edu.au; kush@ee.newcastle.edu.au).

S. Mousavi and U. Valdek are with the Ångström Laboratory, Uppsala University, SE-751 21, Uppsala, Sweden (e-mail: Saed.Mousavi@angstrom.uu.se; Urmas.Valdek@angstrom.uu.se).

T. Söderström is with the Department of Information Technology, Uppsala University, SE-75105 Uppsala, Sweden (e-mail: Torsten.Soderstrom@it.uu.se).

Digital Object Identifier 10.1109/TCST.2005.857405

[1]In some literature $\hat{\sigma}(\omega)$ is used to denote the frequency domain function associated to the time domain function $\sigma(t)$. However, it is another common practice to use $\hat{x}$ to denote an estimate of x. Hence, to maintain clarity of notations we use $\sigma'(\omega)$, etc, to denote the Fourier transform of $\sigma(t)$ etc.

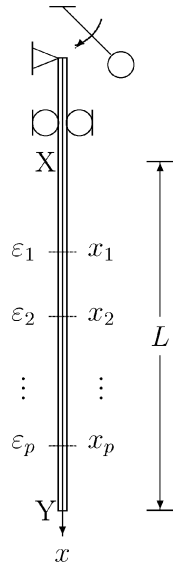

Fig. 1. Transversal wave experimental set up.

is commonly known as the complex Young's modulus. Since $Y(t)$ is a real valued causal function of t, the real part of $\mathcal{E}_\omega$ is an even function of ω and the imaginary part is an odd function of ω [3]. Although the model descriptions (1) and (2) are equivalent, the frequency domain representation (2) is more convenient to use when short time data (frequency range of interest is above 10 Hz) are employed to characterize the dynamic behavior of a viscoelastic material. This brief concerns the determination of complex Young's modulus from flexural wave propagation experiments. Such an experiment is useful when the frequencies of interest are between 10 Hz and 1 kHz.

The experimental setup is described in Fig. 1. A beam is mounted vertically, and is clamped at the top. It is supported by a roller support which prohibits any rigid body motion in the horizontal direction. The specimen is impacted laterally by a pendulum released from a given height (larger the height, more is the impulsive force) giving rise to flexural waves travelling along the bar. The strains due to the wave propagation are registered using strain gauges at sections $\{x_i\}_{i=1}^{p}$ within the beam segment under consideration. The measured signal is proportional to the *bending moment* at the measurement section. The analog strain data are passed through an anti-aliasing filter and discretized. The discretized data are subjected to discrete Fourier transform (DFT) to get a frequency-domain description [3]. A nonparametric identification of the complex modulus is carried out for each frequency. Similar approaches for evaluating material parameters can also be found in [4]–[6].

In [4] and [6], the problem of estimating the complex modulus from flexural wave propagation experiments was considered, where a variable projection problem was solved to compute the complex modulus. The primary aim in this work is to incorporate the additional information hidden in the boundary conditions in the estimation process. As a result we must solve a constrained variable projection problem. Incorporation of the additional information brings in significant improvement in the estimation accuracy [7]. This can also be interpreted as a regularization procedure. The estimation accuracy will also be quantified in terms of the variance of the estimates. Here we start with a brief review of flexural wave dynamics in Section II. Next, we describe the conventional nonlinear least squares estimation of the complex modulus from flexural wave propagation experiments in Section III. Then the algorithm will be modified using the knowledge of the boundary conditions in Section IV. A statistical analysis of the estimation accuracy will also be presented in this section. The analytical results will be validated through experimental study in Section V. We conclude in Section VI.

II. Transverse Waves in a Beam

In a beam propagated by transverse waves, the bending moment $m(x,t)$ and the shear force $q(x,t)$ at any section x and time t are related to the rotational velocity, $\dot{\phi}(x,t)$, and the time derivative of the center-line deflection, $\dot{w}(x,t)$ [4], [8]. These quantities constitute the state vector

$$\mathbf{s}(x,t) = \left[q(x,t) \quad \dot{w}(x,t) \quad m(x,t) \quad \dot{\phi}(x,t)\right]^\top. \quad (4)$$

The dynamics of the state vector are more conveniently expressed in the frequency domain, where the convolutions are transformed to multiplication and the underlying partial differential equations are transformed to ordinary differential equations. We shall consider the Timoshenko beam theory.[2] Here we omit the details and state the frequency domain relationships straightaway. Let the beam have a cross-sectional area A, density ρ and complex Young's modulus $\mathcal{E}_\omega$. In the frequency domain, the state vector follows a system of ordinary differential equations in x [4] given by

$$q'_x(x,\omega) = \mathrm{i}\omega\rho A\dot{w}'(x,\omega) \quad (5)$$

$$\dot{w}'_x(x,\omega) = \frac{\mathrm{i}\omega\psi(\omega)}{A\mathcal{E}_\omega}q'(x,\omega) - \dot{\phi}'(x,\omega) \quad (6)$$

$$m'_x(x,\omega) = q'(x,\omega) + \mathrm{i}\omega\rho I\dot{\phi}'(x,\omega) \quad (7)$$

$$\dot{\phi}'_x(x,\omega) = \frac{\mathrm{i}\omega}{I\mathcal{E}_\omega}m'(x,\omega) \quad (8)$$

where the first-order derivative of a function f with respect to x is denoted by f_x. The second-order derivative with respect to x is denoted by f_{xx}, and so on. Note that, we have introduced

$$\psi(\omega) := \frac{2}{\kappa}\{1+\nu(\omega)\} \quad (9)$$

where $\nu(\omega)$ is the frequency dependent Poisson's ratio and κ is a dimensionless quantity. The value of κ depends upon the cross-sectional geometry [4] of the beam. We have $\kappa = 0.9$ for a circular cross section. The relations (5)–(8) constitute a first-order system of ordinary differential equations of dimension four. The characteristic equation for this system is given by [4]

$$\gamma^4(\omega) + 2a(\omega)\gamma^2(\omega) - b(\omega) = 0 \quad (10)$$

where

$$a(\omega) = \frac{\rho\omega^2}{2\mathcal{E}_\omega}[1+\psi(\omega)] \quad (11)$$

$$b(\omega) = \frac{\rho\omega^2}{\mathcal{E}_\omega}\left[\frac{A}{I} - \frac{\rho\omega^2}{\mathcal{E}_\omega}\psi(\omega)\right]. \quad (12)$$

It is readily verified that the roots of the (10) satisfy

$$\gamma_1^2(\omega) = -a(\omega) + \sqrt{a^2(\omega)+b(\omega)} \quad (13)$$

$$\gamma_2^2(\omega) = -a(\omega) - \sqrt{a^2(\omega)+b(\omega)} \quad (14)$$

which are commonly known as the wave propagation functions. As a consequence the general solution to the bending moment $m'(x,\omega)$ is given by

$$m'(x,\omega) = c_1^+(\omega)\mathrm{e}^{-\gamma_1(\omega)x} + c_2^+(\omega)\mathrm{e}^{-\gamma_2(\omega)x} + c_1^-(\omega)\mathrm{e}^{\gamma_1(\omega)x} + c_2^-(\omega)\mathrm{e}^{\gamma_2(\omega)x}. \quad (15)$$

The quantities $\{c_i^+(\omega)\}_{i=1}^2$ and $\{c_i^-(\omega)\}_{i=1}^2$ depend upon the boundary conditions. Note that $m'(x,\omega)$ is composed of the contributions of two different waves corresponding to the propagation functions $\gamma_1(\omega)$ and $\gamma_2(\omega)$.

III. Least Squares Estimation

As a first step of least squares estimation, a low rank signal model is constructed using the physics of wave propagation described in Section II. The frequency domain measurement $\varepsilon'(x_i,\omega)$ at section x_i and frequency ω is given by

$$\varepsilon'(x_i,\omega) = \varepsilon'_0(x_i,\omega) + \tilde{\varepsilon}'(x_i,\omega) \quad (16)$$

where $\varepsilon'_0(x_i,\omega)$ is the true strain proportional to the bending moment $m'(x_i,\omega)$. The contribution of the measurement noise is given by $\tilde{\varepsilon}'(x_i,\omega)$. The strain is measured at sections $x = x_i$ for $i = 1,\ldots,p$, where $p \geq 5$. Introduce

$$\boldsymbol{\varepsilon}_{\omega 0} = \left[\varepsilon'_0(x_1,\omega) \quad \cdots \quad \varepsilon'_0(x_p,\omega)\right]^\top \quad (17)$$

$$\tilde{\boldsymbol{\varepsilon}}_\omega = \left[\tilde{\varepsilon}'(x_1,\omega) \quad \cdots \quad \tilde{\varepsilon}'(x_p,\omega)\right]^\top \quad (18)$$

$$\boldsymbol{\varepsilon}_\omega = \boldsymbol{\varepsilon}_{\omega 0} + \tilde{\boldsymbol{\varepsilon}}_\omega. \quad (19)$$

It is also important to characterize the statistical properties of the measurement noise in frequency domain. Assume that the noise sequence at the sensors are independent and identically distributed and the spectral density of the distribution exists at each frequency ω. Denote the spectral density at frequency ω by λ_ω. Assume also that the number of data samples (at each sensor) N in time domain is large. Then it can be shown that [6], [9], [10] $\tilde{\boldsymbol{\varepsilon}}_\omega$ is asymptotically[3] $(N \to \infty)$ complex Gaussian distributed with a covariance matrix $\lambda_\omega\mathbf{I}_p$, where $\mathbf{I}_p$ denotes the identity matrix of order p, so that

$$\mathbf{E}\tilde{\boldsymbol{\varepsilon}}_\omega\tilde{\boldsymbol{\varepsilon}}_\omega^* = \lambda_\omega\mathbf{I}_p, \quad \mathbf{E}\tilde{\boldsymbol{\varepsilon}}_\omega\tilde{\boldsymbol{\varepsilon}}_\omega^\top = \mathbf{0} \quad (20)$$

[2]Another and more simplified theory is well known as the Euler–Bernoulli beam theory [8].

[3]We emphasize that $N \to \infty$ is not a strong assumption. In a practical experimental scenario, the value of N is typically 2^{15}. For such high values of N the result can be assumed to be true for all practical purposes.

for every discrete frequency ω. Note that we use $\mathbf{E}$ to denote the mathematical expectation operator. Furthermore, the expressions (20) hold for any finite N if the noise sequences are temporally white. Using (15), (17) we can write the true strain vector $\boldsymbol{\varepsilon}_{\omega 0}$ as

$$\boldsymbol{\varepsilon}_{\omega 0} = \boldsymbol{\Psi}(\mathbf{x}, \mathcal{E}_\omega)\mathbf{c}_\omega \tag{21}$$

where

$$\boldsymbol{\Psi}(\mathbf{x}, \mathcal{E}_\omega) = \begin{bmatrix} \mathrm{e}^{-\gamma_1(\omega)x_1} & \mathrm{e}^{\gamma_1(\omega)x_1} & \mathrm{e}^{-\gamma_2(\omega)x_1} & \mathrm{e}^{\gamma_2(\omega)x_1} \\ \vdots & \vdots & \vdots & \vdots \\ \mathrm{e}^{-\gamma_1(\omega)x_p} & \mathrm{e}^{\gamma_1(\omega)x_p} & \mathrm{e}^{-\gamma_2(\omega)x_p} & \mathrm{e}^{\gamma_2(\omega)x_p} \end{bmatrix} \tag{22}$$

is a $p \times 4$ matrix and $\mathbf{c}_\omega$ is a 4×1 vector given by

$$\mathbf{c}_\omega = k \begin{bmatrix} c_1^+(\omega) & c_1^-(\omega) & c_2^+(\omega) & c_2^-(\omega) \end{bmatrix}^\top \tag{23}$$

and k is the proportionality constant between $m'(x,\omega)$ and $\varepsilon_0'(x,\omega)$. The expression (21) can now be combined with (19) to get

$$\boldsymbol{\varepsilon}_\omega = \boldsymbol{\Psi}(\mathbf{x}, \mathcal{E}_\omega)\mathbf{c}_\omega + \tilde{\boldsymbol{\varepsilon}}_\omega. \tag{24}$$

In (24) we see that the noise-free part of $\boldsymbol{\varepsilon}_\omega$ always lies in the subspace spanned by the columns of $\boldsymbol{\Psi}(\mathbf{x}, \mathcal{E}_\omega)$ for all $\mathbf{c}_\omega$. This provides us with a low rank signal model, which can be exploited for the estimation purpose. One way to do so is to use the least squares estimate [6]

$$\begin{aligned} \hat{\mathcal{E}}_\omega &= \arg\min_{\mathcal{E}} \left\{ \min_{\mathbf{c}} \|\boldsymbol{\varepsilon}_\omega - \boldsymbol{\Psi}(\mathbf{x}, \mathcal{E})\mathbf{c}\|^2 \right\} \\ &= \arg\min_{\mathcal{E}} \boldsymbol{\varepsilon}_\omega^*(\mathbf{x}) \boldsymbol{\Pi}_{\boldsymbol{\Psi}}^\perp(\mathbf{x}, \mathcal{E}) \boldsymbol{\varepsilon}_\omega(\mathbf{x}) \end{aligned} \tag{25}$$

where

$$\boldsymbol{\Pi}_{\boldsymbol{\Psi}}^\perp(\mathbf{x}, \mathcal{E}) = \mathbf{I}_p - \boldsymbol{\Psi}(\mathbf{x}, \mathcal{E}) \left[\boldsymbol{\Psi}^*(\mathbf{x}, \mathcal{E})\boldsymbol{\Psi}(\mathbf{x}, \mathcal{E})\right]^{-1} \boldsymbol{\Psi}^*(\mathbf{x}, \mathcal{E}) \tag{26}$$

is the projection operator onto the nullspace of $\boldsymbol{\Psi}^*(\mathbf{x}, \mathcal{E})$. The basic idea is to project the measurement vector onto the nullspace of $\boldsymbol{\Psi}^*(\mathbf{x}, \mathcal{E})$ and tune $\mathcal{E}$ to minimize the length of the projection. Note that in absence of any more information the estimate (25) can be shown to be the maximum likelihood estimate. A statistical analysis of this estimator was presented in [6]. The main problem with this estimator is the fact that the optimization problem can often be ill-conditioned. During the evaluation of the loss function in (25) numerical problems are encountered quite often. This problem can be solved to a large extent by using a regularization method suggested in [6], where individual columns of $\boldsymbol{\Psi}(\mathbf{x}, \mathcal{E})$ are appropriately scaled to get a numerically well-conditioned matrix. The method described in the following section can also be seen as a regularization to the optimization problem. In this case, additional relations due to boundary conditions are used to improve the numerical properties of the algorithm.

IV. Using the Boundary Conditions

During the experiment design it is sometimes possible to set up the experiment such that one of the boundaries of the beam segment under consideration can be set free. For different types of supports, *clamping*, *pinning* or *roller* for example, there exist ideal boundary conditions [8], but it is very difficult to realize these *ideal* conditions in practice. However, the *free* boundary condition can be realized in laboratory experiments, if proper precaution is taken. The setup depicted in Fig. 1 has been designed specially such that the lower end Y is set free. The upper boundary X is supported through a roller support. As mentioned earlier, it is not advisable to use the *ideal* boundary conditions for the upper end, since these are not realizable exactly. However, a free boundary Y can be used. Let us set $x = 0$ at the free end Y, we have

$$m(0,t) = 0, \quad q(0,t) = 0 \tag{27}$$

where $m(x,t)$ and $q(x,t)$ denote the bending moment and shear force at section x and time t. Recall that the measured signal for a flexural wave experiment is proportional to the bending moment. Thus, from the first boundary condition on the bending moment we get from (15)

$$c_1^+(0,\omega) + c_1^-(0,\omega) + c_2^+(0,\omega) + c_2^-(0,\omega) = 0. \tag{28}$$

To examine the second condition of (27) it is required to express the shear force $q'(x,\omega)$ in terms of $m'(x,\omega)$. In what follows next, we shall omit the arguments of the variables for simplicity. First we shall eliminate ϕ' and q' from (5), (7) and (8). Differentiating (7) with respect to x and combining with (8) we get

$$m'_{xx} = q'_x - \frac{\rho\omega^2}{\mathcal{E}_\omega} m' = q'_x + \gamma_l^2 m' = \mathrm{i}\omega\rho A \dot{w}' + \gamma_l^2 m' \tag{29}$$

where we have used (5) and

$$\gamma_l^2 = -\frac{\rho\omega^2}{\mathcal{E}_\omega}. \tag{30}$$

Eliminating ϕ' from (6) and (7) one gets

$$\begin{aligned} q' &= m'_x - \mathrm{i}\omega\rho I\dot{\phi}' = m'_x + \mathrm{i}\omega\rho I\dot{w}'_x - \frac{I}{A}\psi\gamma_l^2 q' \\ &\Rightarrow \left\{\frac{A}{I} + \psi\gamma_l^2\right\} q' = \frac{A}{I} m'_x + \mathrm{i}\omega\rho A\dot{w}'_x. \end{aligned} \tag{31}$$

Now, we eliminate $\dot{w}'$ from (29) and (31). We differentiate (29) with respect to x and subtract from (31). We have

$$\left\{\frac{A}{I} + \psi\gamma_l^2\right\} q' = m'_{xxx} + \left\{\frac{A}{I} - \gamma_l^2\right\} m'_x \tag{32}$$

which we write as

$$\begin{aligned} \frac{d^3 m'(x,\omega)}{dx^3} + \left\{\frac{A}{I} - \gamma_l^2(\omega)\right\} \frac{dm'(x,\omega)}{dx} \\ = \left\{\frac{A}{I} + \gamma_l^2(\omega)\psi(\omega)\right\} q'(x,\omega). \end{aligned} \tag{33}$$

Using the second boundary condition in (27) we get from (33)

$$\frac{d^3 m'(0,\omega)}{dx^3} + \left\{\frac{A}{I} - \gamma_l^2(\omega)\right\} \frac{dm'(0,\omega)}{dx} = 0. \tag{34}$$

Recall that the strain $\varepsilon_0'(x,\omega)$ is directly proportional to the bending moment $m'(x,\omega)$. Therefore, using (34) and (30) it follows that:

$$\frac{d^3 \varepsilon_0'(0,\omega)}{dx^3} + \left\{\frac{A}{I} + \frac{\rho\omega^2}{\mathcal{E}_\omega}\right\} \frac{d\varepsilon_0'(0,\omega)}{dx} = 0. \tag{35}$$

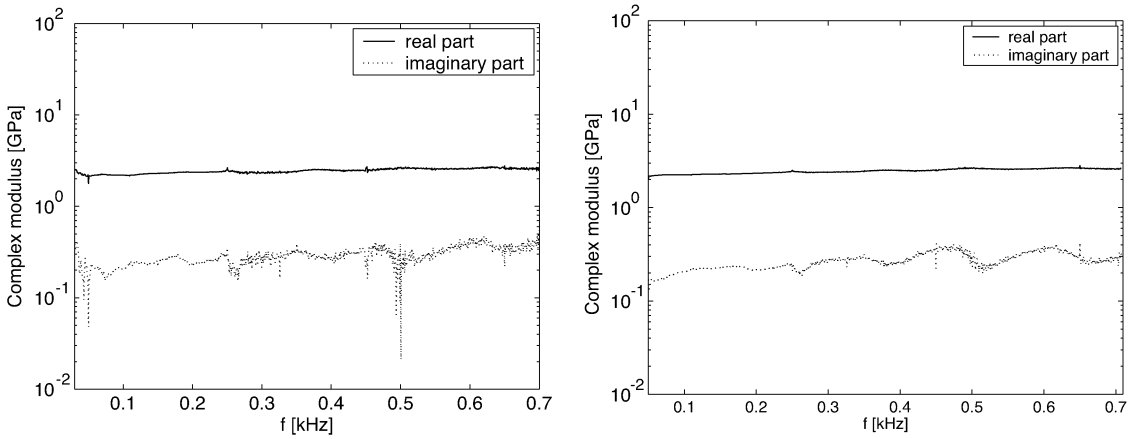

Fig. 2. Mean value of the estimated complex modulus $\mathcal{E}_\omega$ as a function of frequency.

After a few steps of straightforward calculations using (15) and (35) we get

$$\left(c_1^+ - c_1^-\right)\left\{\gamma_1^2 + \frac{\rho\omega^2}{\mathcal{E}_\omega} + \frac{A}{I}\right\}\gamma_1 + \left(c_2^+ - c_2^-\right)\left\{\gamma_2^2 + \frac{\rho\omega^2}{\mathcal{E}_\omega} + \frac{A}{I}\right\}\gamma_2 = 0. \quad (36)$$

From the previous discussion, we can see that the linear constraint on $\mathbf{c}_\omega$ originating from the boundary conditions can be put in the following general form:

$$\mathbf{U}^*\{\mathcal{E}_\omega\}\mathbf{c}_\omega = \mathbf{0}_{n\times 1} \quad (37)$$

where $\mathbf{U}^*\{\mathcal{E}_\omega\}$ is a 2×4 matrix. From (28) and (36), we have

$$\mathbf{U}^*\{\mathcal{E}_\omega\} = \begin{bmatrix} 1 & \left\{\gamma_1^2(\omega) + \frac{\rho\omega^2}{\mathcal{E}_\omega} + \frac{A}{I}\right\}\gamma_1(\omega) \\ 1 & -\left\{\gamma_1^2(\omega) + \frac{\rho\omega^2}{\mathcal{E}_\omega} + \frac{A}{I}\right\}\gamma_1(\omega) \\ 1 & \left\{\gamma_2^2(\omega) + \frac{\rho\omega^2}{\mathcal{E}_\omega} + \frac{A}{I}\right\}\gamma_2(\omega) \\ 1 & -\left\{\gamma_2^2(\omega) + \frac{\rho\omega^2}{\mathcal{E}_\omega} + \frac{A}{I}\right\}\gamma_2(\omega) \end{bmatrix}^\top. \quad (38)$$

Therefore, in order to take the boundary conditions in account, we should solve the optimization problem (25) subject to the constraint (37). To solve the optimization (25) subject to (37) we need at least three measurement sections compared to five sections for the unconstrained problem. This is because of the two additional relationships which are available from the free boundary conditions.

Note from the constraint (37) that $\mathbf{c}_\omega$ belongs to the nullspace of $\mathbf{U}^*(\mathcal{E}_\omega)$. Therefore, it is of interest to parameterize the nullspace of $\mathbf{U}^*(\mathcal{E}_\omega)$. That would mean that we need to construct a 4×2 matrix $\mathbf{V}\{\mathcal{E}_\omega\}$ such that

$$\mathbf{U}^*\{\mathcal{E}_\omega\}\mathbf{V}\{\mathcal{E}_\omega\} = \mathbf{0}_{n\times n}. \quad (39)$$

Hence, from (37) we see that $\mathbf{c}_\omega$ belongs to the column space of $\mathbf{V}\{\mathcal{E}_\omega\}$. This means that there exists a 2×1 vector $\check{\mathbf{c}}_\omega$ such that

$$\mathbf{c}_\omega = \mathbf{V}(\mathcal{E}_\omega\}\check{\mathbf{c}}_\omega. \quad (40)$$

Note that $\mathbf{V}\{\mathcal{E}_\omega\}$ is not unique, and therefore $\check{\mathbf{c}}_\omega$ depends upon the choice of $\mathbf{V}(\mathcal{E}_\omega)$. One possible choice of $\mathbf{V}(\mathcal{E}_\omega)$ is given by

$$\mathbf{V}\{\mathcal{E}_\omega\} = \begin{bmatrix} 1 & \left\{\gamma_2^2(\omega) + \frac{\rho\omega^2}{\mathcal{E}_\omega} + \frac{A}{I}\right\}\gamma_2(\omega) \\ 1 & -\left\{\gamma_2^2(\omega) + \frac{\rho\omega^2}{\mathcal{E}_\omega} + \frac{A}{I}\right\}\gamma_2(\omega) \\ -1 & -\left\{\gamma_1^2(\omega) + \frac{\rho\omega^2}{\mathcal{E}_\omega} + \frac{A}{I}\right\}\gamma_1(\omega) \\ -1 & \left\{\gamma_1^2(\omega) + \frac{\rho\omega^2}{\mathcal{E}_\omega} + \frac{A}{I}\right\}\gamma_1(\omega) \end{bmatrix} \quad (41)$$

for which we can readily verify (39). Now using (40) we can rewrite the constrained optimization problem in a more convenient form. Using (40) in (25) we see that the constrained problem can be reduced to an equivalent unconstrained problem where a modified estimate $\hat{\mathcal{E}}_\omega^c$ is obtained

$$\begin{aligned}\hat{\mathcal{E}}_\omega^c &= \arg\min_{\mathcal{E}}\left\{\min_{\check{\mathbf{c}}} \|\boldsymbol{\varepsilon}_\omega - \boldsymbol{\Upsilon}(\mathbf{x},\mathcal{E})\check{\mathbf{c}}\|^2\right\} \\ &= \arg\min_{\mathcal{E}} \boldsymbol{\varepsilon}_\omega^*(\mathbf{x})\boldsymbol{\Pi}_{\boldsymbol{\Upsilon}}^{\perp}(\mathbf{x},\mathcal{E})\boldsymbol{\varepsilon}_\omega(\mathbf{x}) \end{aligned} \quad (42)$$

where

$$\boldsymbol{\Upsilon}\{\mathcal{E}_\omega\} = \boldsymbol{\Psi}(\mathbf{x},\mathcal{E}_\omega)\mathbf{V}\{\mathcal{E}_\omega\}. \quad (43)$$

The accuracy of the parameter estimates improves significantly when boundary conditions are employed in the estimation process. They can be seen as extra noise-free measurements [11]. These boundary conditions bring in more precise information regarding the *nuisance* parameter $\mathbf{c}_\omega$ that it is orthogonal to the space spanned by the columns of $\mathbf{U}(\mathcal{E}_\omega)$. Hence, the dimension of the search space is reduced by two. As a result, in (42) we minimize the orthogonal projection of $\boldsymbol{\varepsilon}_\omega$ onto a subspace of dimension $p-2$ compared to $p-4$ in (25). This increase makes the modified algorithm more robust to the additive noise compared to the case when the constraints are not used. This can also be seen as a regularization to the original numerically ill-conditioned problem, which improves the conditioning of the problem.

Next, we give the expressions for the covariance matrices of the estimates. Introduce

$$\boldsymbol{\Phi}(\mathcal{E}_\omega) = \frac{\partial\boldsymbol{\Psi}(\mathcal{E}_\omega)}{\partial\mathcal{E}_\omega}\mathbf{c}_\omega \quad (44)$$

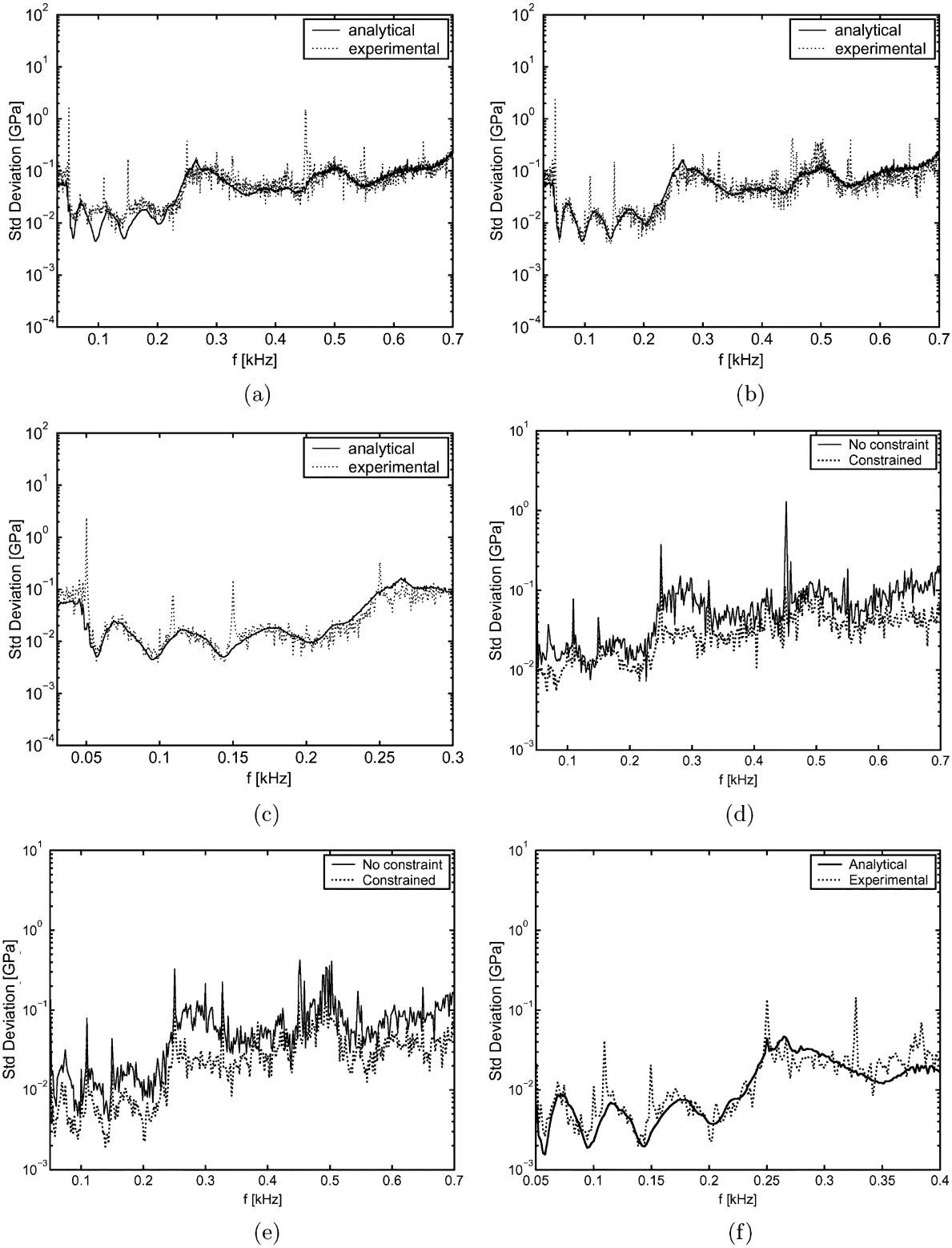

Fig. 3. Analytical S.D. and experimental S.D. of the estimated complex modulus. (a), (b) Comparison between the analytical and the experimental S.D. of the unconstrained estimate of the complex modulus $\mathcal{E}_\omega$. (c) Zoomed version of (b). (d), (e) Comparison between the experimental S.D. of the constrained and unconstrained estimates. (f) Comparison between the analytical and the experimental S.D. of the imaginary part of the constrained estimate.

$$\boldsymbol{\Phi}'(\mathcal{E}_\omega) = \frac{\partial \mathbf{U}^*(\mathcal{E}_\omega)}{\partial \mathcal{E}_\omega}\mathbf{c}_\omega \tag{45}$$

$$\check{\boldsymbol{\Phi}}(\mathcal{E}_\omega) = \boldsymbol{\Phi}(\mathcal{E}_\omega) - \boldsymbol{\Psi}(\mathbf{x},\mathcal{E}_\omega)\mathbf{U}\{\mathcal{E}_\omega\} \times \left[\mathbf{U}^*\{\mathcal{E}_\omega\}\mathbf{U}\{\mathcal{E}_\omega\}\right]^{-1}\boldsymbol{\Phi}'(\boldsymbol{\alpha}_\omega). \tag{46}$$

Then it was shown in [6] that $\hat{\mathcal{E}}_\omega$ is complex Gaussian with variance

$$\mathrm{Var}(\hat{\mathcal{E}}_\omega) = \lambda_\omega \left[\boldsymbol{\Phi}^*(\mathcal{E}_\omega)\boldsymbol{\Pi}_{\boldsymbol{\Psi}}^{\perp}\{\mathbf{x},\mathcal{E}_\omega\}\boldsymbol{\Phi}(\mathcal{E}_\omega)\right]^{-1}. \tag{47}$$

Furthermore, it has been shown in [12] that the constrained estimate $\hat{\mathcal{E}}_\omega^c$ is also complex Gaussian with variance

$$\mathrm{Var}\left(\hat{\mathcal{E}}_\omega^c\right) = \lambda_\omega \left[\check{\mathbf{\Phi}}^*(\mathcal{E}_\omega)\mathbf{\Pi}_{\mathbf{\Upsilon}}^{\perp}\{\mathcal{E}_\omega\}\check{\mathbf{\Phi}}(\mathcal{E}_\omega)\right]^{-1}. \quad (48)$$

Regarding the relative quality of the estimates $\hat{\mathcal{E}}_\omega$ and $\hat{\mathcal{E}}_\omega^c$ it was also shown in [12] that

$$\mathrm{Var}\left(\hat{\mathcal{E}}_\omega^c\right) \leq \mathrm{Var}(\hat{\mathcal{E}}_\omega). \quad (49)$$

In fact, (49) is valid even if the noise at different sensors are correlated to each other [12].

V. Experimental Results

The analytical results were applied to experimental data, where a polypropylene beam specimen of length 1.5 m with uniform circular cross section was considered. The density ρ of polypropelene is 915 $\mathrm{kg/m^3}$ and the Poisson's ratio ν is 0.33 [13]. The recorded analog strain signals were sampled at 20 kHz, i.e., the corresponding value of the sampling interval $T = 5\ \mu$s. The positions $\{x_i\}_{i=1}^p$ of the sensors were taken as

$$\mathbf{x} = \begin{bmatrix} 0.102 \\ 0.348 \\ 0.468 \\ 0.685 \\ 0.870 \\ 1.003 \\ 1.147 \\ 1.300 \end{bmatrix}^\top \quad (50)$$

where the coordinates are expressed in meters. The number of samples collected from each channel was $N = 2^{15}$. With this choice of N we can use the computationally efficient radix-2 fast Fourier transform (FFT) algorithm [3] to compute DFT. With these values of N and T we have a resolution of 0.611 Hz in the frequency domain. At the beginning of each interval of measurement, the tested beam was at rest, and at the end the signals were reduced almost to the level of the noise. This ensures that the signals could be transferred to the frequency domain by the FFT algorithm without the use of any window technique.

The experiment was repeated ten times to obtain ten statistically independent data sets. The results of the identification is plotted in Fig. 2, where the variation of the real part and the imaginary part of the estimated complex modulus, each as a function of frequency, are shown. The results given in Fig. 2(a) were obtained when the boundary conditions were *not* used in the estimation algorithm. When the boundary conditions at the free end were used, the results shown in Fig. 2(b) were obtained. In each case, the value of the complex modulus at each frequency was obtained by averaging the results of ten independent experiments. As can be seen in Fig. 2, the use of the free end boundary conditions leads to improved estimates, in the sense that there is a significant noise reduction in the estimates. This is due to two reasons. First, unlike the estimates in Fig. 2(a), the estimates in Fig. 2(b) do not suffer from numerical problems [see for example the noisy estimates around 500 Hz in Fig. 2(a)]. Second, the standard deviations of the estimates in Fig. 2(b) are significantly smaller than those in Fig. 2(a).

In order to check the validity of the expression given by (47), the analytical standard deviation was compared with the sample standard deviation obtained from the ten independent experiments. The result of such a comparison is shown in Fig. 3(a) (b). Note that the noise spectral density λ_ω is unknown. If the noise is white, the analytical variance (47) obtained using an arbitrary value of the noise variance is directly proportional to the actual variance of the estimates, which should be reflected as a constant difference in a semilog scale. The value of λ_ω used in the calculation of the analytical variance (47) is 0.56×10^{-8} for all ω. It can be seen in Fig. 3(a) and (b) that the theoretical prediction using (47) is very well in accordance with the results obtained from the experiments. Let us now focus on the results in Fig. 3(c), where we have shown a zoomed version of Fig. 3(b). A close inspection reveals that the analytical standard deviation is significantly low in comparison to the experimental standard deviation at frequencies which are close to 50, 100, 150, and 250 Hz. This proves the presence of strong 50 Hz power line interference. Next, we compare the standard deviation of the constrained estimate (which uses the boundary conditions at the free end) with the standard deviation of the unconstrained estimate in Fig. 3(d) and (e). In Fig. 3(d), we have compared the standard deviations of the real parts of the complex modulus estimates. A similar comparison for the imaginary part is shown in Fig. 3(e). Here we see that the constrained estimate always outperforms the unconstrained estimate. The validity of the expression (48) is checked in Fig. 3(f), where the experimental standard deviation of the imaginary part of the constrained complex modulus estimate is compared with the analytically predicted standard deviation.[4] It can be seen that the experimental standard deviation is very well in accordance with the analytical prediction. Finally, in Fig. 3(a), (b), (d), and (e) we see that the standard deviation of the estimates increases rapidly with frequency. This indicates that the excitation at the higher frequencies is not of sufficient magnitude, and must be improved in order to obtain better estimates at higher frequencies.

VI. Conclusion

In this brief we have considered the estimation of complex Young's modulus from transverse wave experiment. The main goal has been to modify the usual least squares estimate so that additional information provided by the boundary conditions can be incorporated in the estimation algorithm. Special precautions must be taken in designing the experiment so that one boundary can be set free. The main idea presented here is to exploit two additional relationships provided by the boundary conditions at the free boundary. As a result, it is required to solve a constrained least squares problem instead of an unconstrained least squares problem. We have shown that the resulting constrained least squares problem can be reduced to an *equivalent* unconstrained variable projection problem. The resulting estimates are significantly better than the conventional least squares estimate. The expressions for the variances of the estimates are also given. All analytical results are validated using experimental data. The constrained least squares estimate outperforms the unconstrained estimate by a significant margin.

[4]It was not possible to compute the analytical standard deviation of the constrained estimate accurately for the whole frequency range due to numerical problems. Therefore, a part of the frequency range is considered in Fig. 3(f).

REFERENCES

[1] W. Flügge, *Viscoelasticity*, 2nd ed: Springer-Verlag, 1975.

[2] R. S. Lakes, *Viscoelastic Solids*. Boca Raton, FL: CRC, 1999.

[3] A. V. Oppenheim and R. W. Schafer, *Discrete-Time Signal Processing*. Englewood Cliffs, NJ: Prentice-Hall, 1975.

[4] L. Hillström and B. Lundberg, "Analysis of elastic flexural waves in nonuniform beams based on measurement of strains and accelarations," *J. Sound Vib.*, vol. 246, pp. 227–242, 2001.

[5] L. Hillström, M. Mossberg, and B. Lundberg, "Identification of complex modulus from measured strains on an axially impacted bar using least squares," *J. Sound Vib.*, vol. 230, pp. 689–707, 2000.

[6] K. Mahata, S. Mousavi, T. Söderström, M. Mossberg, U. Valdek, and L. Hillström, "On the use of flexural wave propagation experiments for identification of complex modulus," *IEEE Trans. Contr. Syst. Technol.*, vol. 11, no. 6, pp. 863–874, Nov. 2003.

[7] K. Mahata and T. Söderström, "Improved estimation performance using known linear constaints," *Automatica*, vol. 40, no. 8, pp. 1307–1318, 2004.

[8] L. Meirovitch, *Principles and Techniques of Vibrations*. Englewood Cliffs, NJ: Prentice-Hall, 1997.

[9] D. R. Brillinger, *Time Series: Data Analysis and Theory*. New York: Holt, Rinehart and Winston, 1975.

[10] R. Pintelon and J. Schoukens, *System Identification: A Frequency Domain Approach*. Piscataway, NJ: IEEE Press, 2001.

[11] M. Mossberg, L. Hillström, and T. Söderström, "Non-parametric identification of viscoelastic materials from wave propagation experiments," *Automatica*, vol. 37, no. 4, pp. 511–521, Apr. 2001.

[12] K. Mahata, "Estimation using low rank signal models," Ph.D. dissertation, Dept. Inf. Technol., Uppsala University, 2003.

[13] S. Mousavi, D. F. Nicolas, and B. Lundberg, "Identification of complex moduli and Poisson's ratio from measured strains on an impacted bar," *J. Sound Vib.*, vol. 277, no. 4–5, pp. 971–986, Nov. 2004.